Solar Energy Materials & Solar Cells 95 (2011) 933–941

Contents lists available at ScienceDirect

Solar Energy Materials & Solar Cells

journal homepage: www.elsevier.com/locate/solmat

Temperature dependence of polymer/fullerene organic solar cells

W. Bagienski, M.C. Gupta *

Department of Electrical and Computer Engineering, University of Virginia, P.O. Box 400743, 351 McCormick Road, Charlottesville, VA 22904-4743, USA

ARTICLE INFO

Article history:
Received 17 June 2010
Received in revised form
24 November 2010
Accepted 25 November 2010
Available online 8 January 2011

Keywords:
Organic solar cells
P3HT
PCBM
Temperature dependence
Polymer
Fullerene

ABSTRACT

The temperature dependence of bulk heterojunction organic solar cells fabricated from poly(3-hexylthiophene) (P3HT) and [6,6]-phenyl-C_{61}-butyric acid methyl ester (PCBM) was studied in detail. Individual materials as well as blends and solar cell devices were examined. Light absorption, photoluminescence, quantum efficiency, total efficiency, and current–voltage characteristics were studied from temperatures −10 to 140 °C. A method and apparatus for testing these parameters at various temperatures is described. Parameters were measured for both unannealed and annealed samples to give insight into the annealing process. It was found that absorption and photoluminescence of devices shift both position and intensity with varying temperatures. Quantum efficiency and total efficiency were monitored as they increased with annealing. Once annealed, device efficiency peaked at temperatures from 10 to 60 °C because of competing temperature dependent effects of the materials. The temperature dependence study provides valuable information on device properties and thermal annealing.

1. Introduction

In recent years, bulk heterojunction organic solar cells made from conjugated polymers and fullerenes have gained popularity as promising sources of alternative energy due to their low cost, ease of fabrication, flexibility, and light weight [1]. There have been numerous recent demonstrations of roll-to-roll processed organic solar cells and their applications [2–7]. The blend of P3HT and PCBM is one of the most popular and successful material systems with reported efficiencies as high as 7% [8–10]. These efficiencies have been obtained through many studies and optimizations of materials, processing methods, and device configurations. However, organic solar cells are still not suitable for large scale commercialization and further improvements are necessary [8–10].

Until recently, organic solar cells have typically been made on the small scale on glass substrates in laboratory settings. They are now coming closer to reaching their potential with the demonstration of roll-to-roll processed devices on flexible substrates (including ITO free) [2–4], round robin studies [11], and large area grid connected devices [6]. A potential organic solar cell product was recently demonstrated and tested by Krebs et al. [5]. Flexible organic solar cells were made using roll-to-roll processing and integrated into a device, including white LED light and a rechargeable battery to provide lighting for people in Zambia, Africa. While they showed it was possible to meet a small scale lighting need, the product still needed further improvements and cost reduction to be a viable commercial product.

Several alternative approaches to organic solar cells are being considered. A review of the current state of organic photovoltaics along with promising new developments was given by Helgesen et al. in 2010 [12]. They described the possible routes that may lead to significant advancements such as new polymers, polymer/polymer solar cells, thermocleaveable materials, cross-linked polymers, hybrid devices, tandem devices, and ITO free devices. Roll-to-roll processed ITO free thermocleaved solar cells have been reported where high power LEDs were used to selectively thermocleave the active layer [4].

These demonstrations show that organic solar cells are closer than ever to be viable for mass production. A recent cost analysis done on roll-to-roll processed organic photovoltaic devices stated that the cost per unit power was still an order of magnitude higher than that of silicon solar panels [6]. Further improvements are needed in efficiency, cost, and stability for large scale manufacturing. A greater understanding of the materials and devices will lead to higher efficiencies and better stability.

Temperature dependence studies are valuable for organic solar cells because they can give insight into the fundamentals of the devices and materials as well as practical information about device performance in real world conditions. There have been several previous studies on the temperature dependence of P3HT and P3HT/PCBM solar cells. Temperature dependence studies of light absorption of P3HT [13], mobility of P3HT [14–16], photoluminescence of P3HT [17], and total efficiency and *I–V* parameters of P3HT/PCBM devices [12,18] have been reported. While these studies have given insight into P3HT and P3HT/PCBM solar cells, further research work is required to understand the

* Corresponding author. Tel.: +1 434 924 6167; fax: +1 434 924 8818.
E-mail address: mgupta@virginia.edu (M.C. Gupta).

0927-0248/$ - see front matter © 2010 Elsevier B.V. All rights reserved.
doi:10.1016/j.solmat.2010.11.026

various loss mechanisms in organic solar cell devices. To the best of our knowledge, the temperature dependence of PCBM light absorption, P3HT/PCBM blend light absorption, P3HT/PCBM blend photoluminescence, and device quantum efficiency have not been previously studied.

Thermal annealing has been shown to be a critical step in the fabrication of P3HT/PCBM solar cells [19,20]. Often finding the optimal annealing time and temperature requires many devices with many annealing conditions. Differential scanning calorimetry (DSC) has been used to study the glass transition temperature, *crystallinity*, and melting point of P3HT; however, this does not provide a specific annealing temperature for best device performance [21,22]. By studying the temperature dependence of both unannealed and annealed devices in the range of annealing temperatures, we can learn about the annealing process and monitor it as it occurs. Our method allows real time monitoring of devices during the annealing process. This provides an efficient way to optimize annealing in new material systems.

In this study, we compliment the previous studies by providing a more complete picture of the temperature dependence of P3HT/PCBM solar cells. The method and apparatus are described to characterize properties of the materials and devices at various temperatures. Light absorption, photoluminescence, quantum efficiency, and total efficiency were studied from -10 to 140 °C. Temperature dependent measurements were made for unannealed and annealed devices to examine the effect of annealing. Samples were cycled through different temperature transitions to determine if temperature effects were reversible.

2. Materials and methods

Regioregular P3HT with greater than 90% head to tail regiospecific conformation was purchased from Sigma Aldrich. PCBM with purity of 99.5% was purchased from Nano-C. ITO coated glass slides with an antireflection coating and sheet resistance of 8–12 ohms per square were purchased from Delta Technologies. PEDOT dissolved in water was purchased from H.C. Starck.

All samples were fabricated using the following procedure. Pure P3HT and pure PCBM solutions were made by dissolving 10 mg of material in 1 mL of chlorobenzene. P3HT/PCBM blend solutions were made by dissolving 4.5 mg of P3HT and 5.5 mg of PCBM in 1 mL of chlorobenzene. In all cases, the solution was stirred and heated at 65 °C until the material was dissolved, spin coated at 500 rpm for 40 s, dried in still air for 20 min, and then soft baked at 60 °C in a vacuum oven for 30 min to remove any residual solvent. For absorption and photoluminescence measurements, the organic layers were spin coated on quartz substrates. For quantum and total efficiency measurements, devices were fabricated by spin coating a thin (approximately 40 nm) layer of PEDOT on pre-cleaned and patterned ITO coated glass substrates. The PEDOT layer was spun at 4000 rpm for 60 s, dried in air at 110 °C for 15 min, and then the P3HT/PCBM blend was coated on top as stated above, yielding an active layer thickness of approximately 80 nm. Aluminum electrodes 80 nm thick were deposited by electron beam in a high vacuum system (10^{-6} Torr) through a shadow mask. The active device area was approximately 15 mm^2 and was defined by the overlap of the ITO and aluminum. Devices referred to as "annealed" were heated on a hot plate in air at 130 °C for 2 min prior to the experiment. "Unannealed" devices received no heating prior to the experiment, but did get heated during the experiment.

All measurements were made in a small vacuum chamber with two glass viewports and various feedthroughs. The chamber was flushed with nitrogen, partially sealed, and kept under nitrogen flow during the experiment. Samples were mounted in the chamber on a copper plate, which was in contact with a thermoelectric device that was used to heat and cool the samples. Temperature was monitored using a thermocouple inside the copper plate. Temperature was controlled by varying the current supplied to the thermoelectric device. All data were taken through three sequential temperature transitions: heating from -10 to 140 °C, cooling from 140 to -10 °C, and heating again from -10 to 140 °C. Temperature was changed in 10 °C intervals and data was recorded for each temperature. Temperature was held within ± 1 °C during each measurement.

Absorption was measured using an ultraviolet–visible (UV–vis) spectrophotometer. The chamber was placed inside the spectrophotometer, and the light beam was aligned to pass through the sample and the glass viewports. Photoluminescence was measured using a fiber spectrometer. The excitation source used was a 488 nm argon ion laser. A laser power density of approximately 200 mW/cm^2 was used for P3HT/PCBM blends. For P3HT films this was reduced to approximately 8 mW/cm^2 because the photoluminescence intensity was much greater.

Quantum efficiency measurements were made by passing a while light through a monochromator to obtain specific wavelengths. The light was then passed through the glass viewport onto the device in the chamber. For each specific wavelength, the device was illuminated and an *I–V* measurement was taken and recorded. The incident optical power was measured and recorded for each wavelength. External quantum efficiency (defined as the number of electrons output by the device per second divided by the number of incident photons on the device per second) was calculated and plotted at each temperature by comparing the short circuit current to the incident optical power. Total efficiency measurements were made by placing the chamber under a solar simulator that was adjusted to shine 100 mW/cm^2 (one sun) of simulated AM 1.5 white light through the viewport onto the device. *I–V* curves were measured and recorded at each temperature.

Control samples were made to differentiate between the effects of temperature and any other effects that may be present such as time, light exposure, etc. The control samples went through the same procedure as experimental samples, except they were held at room temperature for the entire duration to eliminate the temperature variability.

3. Results

3.1. Absorption

Absorption was measured at intervals of 5 nm wavelength. Control samples did not show any significant change in absorption. Absorption data was corrected to account for the reflection and absorption of the quartz substrates and glass viewports. Scattering losses are estimated to be negligible for the purpose of this work. The absorption data was not corrected for the reflection of the organic films, which should not affect the interpretation of the data.

3.1.1. P3HT

Absorption data for P3HT is shown in Fig. 1. The data shown is for an annealed sample during the second temperature transition (cooling); however, the trend displayed is representative of all of the temperature transitions (heating or cooling cycles) for both unannealed and annealed P3HT. The temperature dependence of P3HT absorption was found to agree with previously reported results [13]. The absorption spectra showed a redshift, increase in peak absorption, and better defined shoulders with decreasing temperature. This is consistent with the view that P3HT polymer chains have smaller conjugation lengths, a broader distribution of conjugation lengths, and more conformational defects at higher temperatures [13]. The absorption shifts towards the blue at higher temperatures because polymers with shorter conjugation lengths

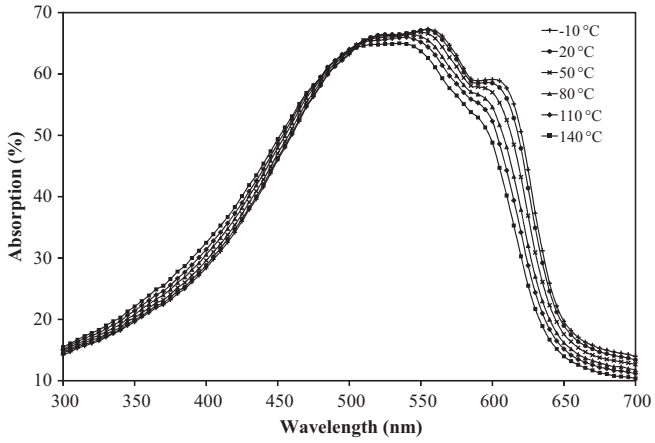

Fig. 1. Unannealed P3HT absorption, second temperature transition, cooling from 140 to −10 °C.

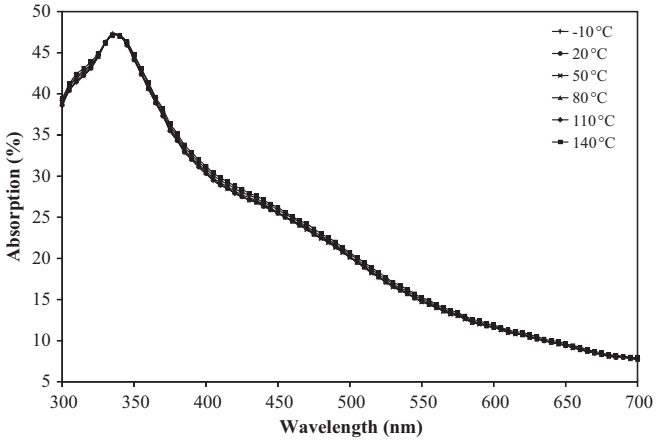

Fig. 2. PCBM absorption, first temperature transition, heating from −10 to 140 °C.

tend to absorb higher energy photons [13]. Unannealed P3HT showed a small increase in absorption after annealing. At −10 °C, the absorption peak was 1.3% higher after annealing. This indicates that some crystallization of P3HT occurred. Literature has also shown that pure P3HT films show a slight increase in absorption after annealing because some disordering occurs during the coating process [23]. After the first heating, unannealed P3HT followed the same trend as annealed P3HT, and the temperature effects were completely reversible during subsequent cooling and heating transitions.

3.1.2. PCBM

Temperature dependent absorption data for PCBM is shown in Fig. 2. There was no significant change in absorption at different temperatures. This indicates that the structure of PCBM does not change with temperature. Since PCBM is a small molecule and stable at these temperatures, one would not expect the change in absorption that polymers like P3HT exhibit. Absorption of PCBM did not show any significant change after annealing, or throughout the various temperature cycles. This is consistent with literature, which has shown that PCBM absorption shows little change after annealing [23]. This indicates that any change in P3HT/PCBM blend absorption will be due to P3HT.

3.1.3. Unannealed P3HT/PCBM blend

Absorption data for the unannealed P3HT/PCBM blend during the first temperature transition (heating) is shown in Fig. 3. At low temperatures, the behavior was like that of pure P3HT, showing a decrease and blueshift of absorption with increasing temperature. Upon reaching temperatures around 90 °C, the behavior changed. When heated above 90 °C the absorption peak increased with temperature. This can be seen in Fig. 4, an enlarged view of the area between 480 and 580 nm of Fig. 3. It is typical for P3HT/PCBM films to show higher absorption after heating due to crystallization of the film [23]. This is apparent in the absorption at 140 °C, which had higher peak absorption near 500 nm than any other temperature. It can be observed that there is a slight shift in the peak near 335 nm, which is not present in the data for pure PCBM and does not follow the trend for pure P3HT. This could be due to changes in the morphology of the blend.

In Fig. 5 the data during the second temperature transition (cooling) after the initial heating is shown. The absorption at 140 °C corresponds to the 140 °C data during the first transition; however, upon cooling all subsequent lower temperatures showed higher absorption than before. This is due to the crystallization that occurred during the first heating cycle. After the sample had been heated, the trend of increasing absorption with lower temperature was restored. The peak absorption at −10 °C after heating was 3% higher than the value at that temperature before heating.

The magnitudes of the absorption peaks in the visible range (near 500 nm) for unannealed P3HT/PBM blend during the first two temperature transitions are plotted in Fig. 6. Three regions can

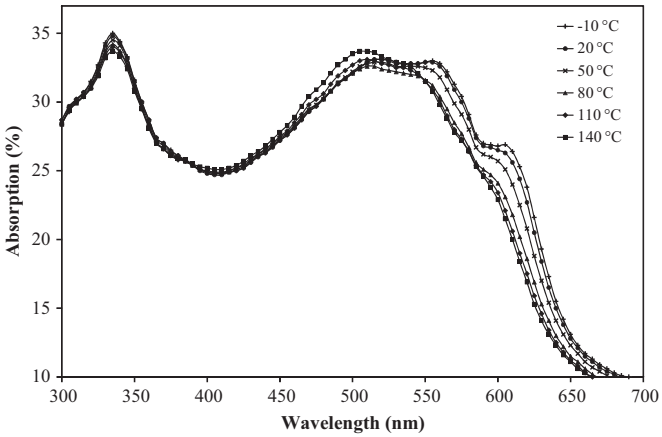

Fig. 3. Unannealed P3HT/PCBM blend absorption, first temperature transition, heating from −10 to 140 °C.

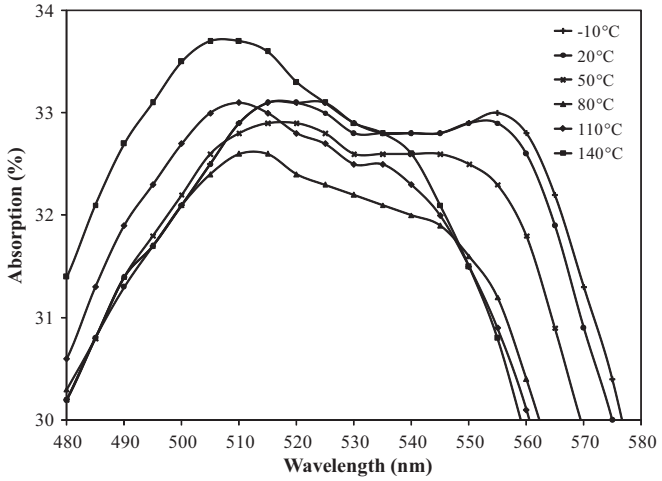

Fig. 4. Unannealed P3HT/PCBM blend absorption, first temperature transition, heating from −10 to 140 °C (enlarged scale).

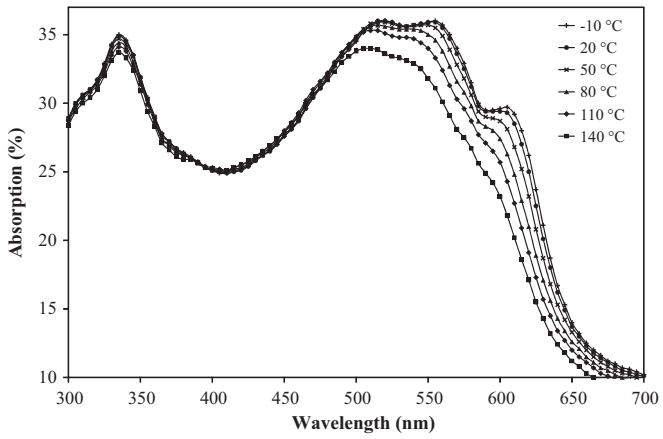

Fig. 5. Unannealed P3HT/PCBM blend absorption, second temperature transition, cooling from 140 to −10 °C.

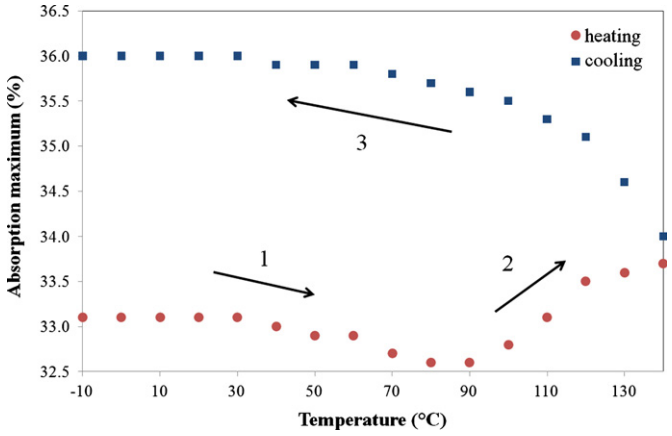

Fig. 6. Behavior of unannealed P3HT/PCBM absorption during first two temperature transitions.

be observed. In the first region, peak absorption decreased with increasing temperature. Once a critical temperature was reached around 80 °C, crystallization began to take place and absorption increased with temperature in the second region. On cooling, the absorption increased permanently for all temperatures and the trend of higher absorption at lower temperatures was restored. The trend in region three was maintained over subsequent temperature changes. Samples that had been annealed prior to the experiment followed the trend in the third region, and the changes with temperature were reversible. The temperature dependence of the annealed P3HT/PCBM blend followed the behavior of pure P3HT, which was expected because PCBM did not show any change with temperature.

3.2. Photoluminescence

Photoluminescence (PL) data was recorded at 2 nm interval. The rise in PL intensity at short wavelengths (below 575–600 nm) was due to the excitation source (488 nm) affecting the data. Control samples showed PL with constant peak positions and intensity variations of less than 5%. At all temperatures, P3HT/PCBM film PL intensities were much lower than pure P3HT PL intensities due to quenching. Photoluminescence of PCBM films could not be observed with the setup; hence, it was not included.

3.2.1. Unannealed P3HT

Photoluminescence data for unannealed P3HT during the first temperature transition (heating) is shown in Fig. 7. The data showed a blueshift and broadening with increase in temperature, which is consistent with literature [17]. There was a decrease in intensity with increasing temperature until around 80 °C, at which the intensity began to rise with increase in temperature. In literature, PL intensity of annealed P3HT films consistently decreased with increasing temperature (temperature range was below room temperature) [17]. The increase in PL at low temperatures was found to be due to higher quantum efficiency of the PL at low temperatures due to less thermally activated non-radiative recombination. The increase in PL intensity at high temperature for the unannealed sample here indicates that the quantum efficiency of PL increases at high temperatures. The reason for the increase at high temperatures is as seen in the absorption data, P3HT becomes more ordered when heated, and this reduces defects and non-radiative recombination. The data shows that crystallization of the film has a greater effect on PL efficiency than the temperature effect alone.

In Fig. 8 the data for the second temperature transition (cooling) is shown. The data now agrees with trends in literature, showing an increase in PL intensity with decreasing temperature [17]. The PL intensities at all temperatures below 140 °C were higher than those in the previous transition, indicating that quantum efficiency of the PL was permanently increased after first heating cycle. This confirms that annealing P3HT permanently increases the PL intensity. The shifts in peak positions remained the same as in the previous transition.

The behavior of the PL intensity maxima during the heating and cooling temperature transitions is shown in Fig. 9. The behavior was very similar to the absorption of the unannealed P3HT/PCBM

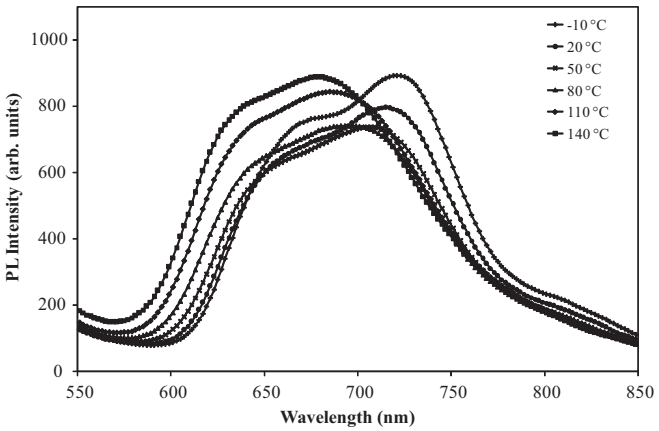

Fig. 7. Unannealed P3HT PL intensity, first temperature transition, heating from −10 to 140 °C.

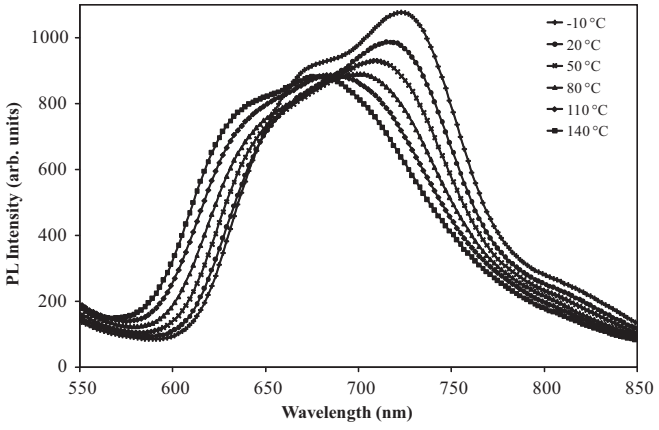

Fig. 8. Unannealed P3HT PL intensity, second temperature transition, cooling from 140 to −10 °C.

blend in Fig. 6. Three regions can be observed: in the first region, PL intensity decreased with increasing temperature. Once a critical temperature was reached, crystallization began to take place and PL intensity increased with temperature in the second region. On cooling, the PL intensity was permanently increased over all temperatures and the trend of higher PL intensity at lower temperatures was restored. Once annealing had taken place, the PL intensity followed the trend in the third region. Samples that were annealed prior to the experiment followed the trend in the third region and the temperature effects were reversible.

3.2.2. Unannealed P3HT/PCBM blend

Photoluminescence data for the unannealed P3HT/PCBM blend during the first temperature transition (heating) is shown in Fig. 10. The shift in peak positions was similar to that of P3HT. Much like unannealed P3HT, the peak PL intensity began to rise above 80 °C. The data suggests that the quantum efficiency of PL improved with annealing, but quenching did not. It appears that the addition of PCBM to P3HT does not affect the temperature dependence of the PL.

In Fig. 11 the data for the second temperature transition (cooling) is shown. On cooling the PL intensity rose above previous levels. This again indicates that annealing did not improve quenching, but it did increase PL intensity. The behavior was similar to that of pure P3HT.

All of the PL data for the unannealed P3HT/PCBM blend show that the PL followed the trends of the pure P3HT films. The behavior during the first two temperature transitions was very similar to that shown in Fig. 9. Heating permanently increases PL intensity.

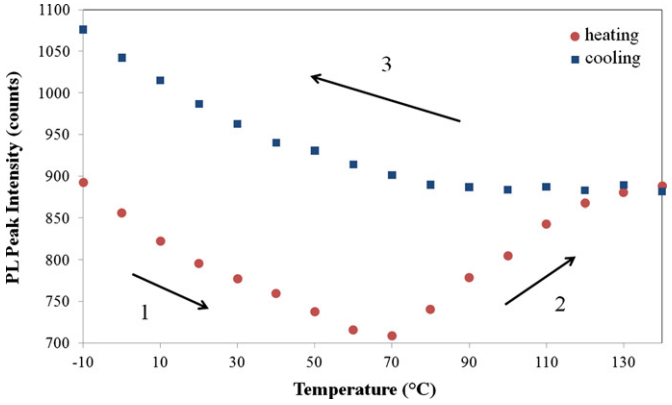

Fig. 9. Behavior of unannealed P3HT photoluminescence during first two temperature transitions.

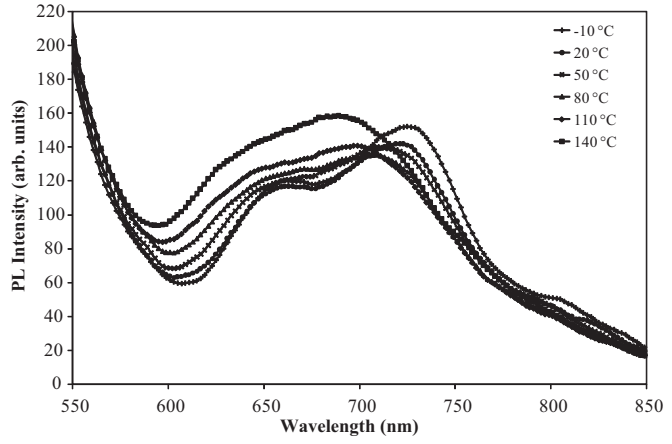

Fig. 10. Unannealed P3HT/PCBM blend PL intensity, first temperature transition, heating from −10 to 140 °C.

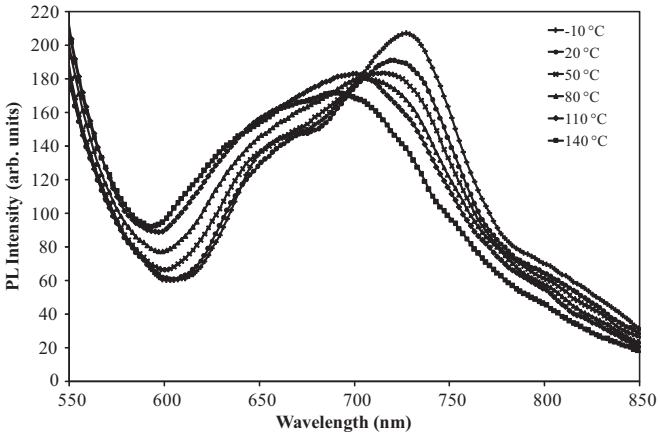

Fig. 11. Unannealed P3HT/PCBM blend PL intensity, second temperature transition, cooling from 140 to −10 °C.

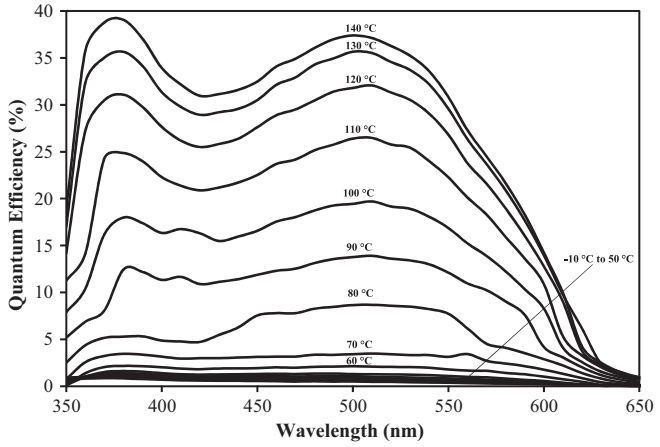

Fig. 12. Unannealed device QE, first temperature transition, heating from −10 to 140 °C.

Once fully annealed, peaks showed reversible shifts in intensity and wavelength. It should be noted that the PL intensity began to rise at a lower temperature than absorption, and continued to rise when changes in absorption were minimal. This leads to the conclusion that the best way to monitor annealing without making full devices is to monitor PL intensity. When the PL ceases to increase upon heating it indicates that crystallization is complete.

3.3. Quantum efficiency

Quantum efficiency (QE) data was taken at 10 nm intervals. Control devices did not show any significant change in quantum efficiency.

3.3.1. Unannealed P3HT/PCBM device

QE data for the unannealed P3HT/PCBM device during the first temperature transition (heating) is shown in Fig. 12. QE was initially very low and began to increase rapidly with increase in temperature around 60 °C. The increase in QE was due to the increased mobility in P3HT due to crystallization. The QE continued to increase after 130 °C, suggesting that 130 °C was not the optimal annealing temperature; however, the improvement in QE at 140 °C compared to 130 °C was relatively small. Also, QE at 360 nm was comparable to the value at 500 nm. At 360 nm, light is primarily absorbed by PCBM as P3HT absorption is very small.

Fig. 13 shows the peak QE (in the visible light range near 500 nm) at each temperature (peaks occurring at different wavelengths). The peak QE began to rise rapidly around 60 °C and continued to rise up to 140 °C. The rapid increase in QE around 70 °C agrees with the changes in the absorption and PL of unannealed samples around the same temperature, showing that the minimum temperature at which crystallization of the films begins to take place is in that range. A plateau may start forming at high temperatures. Though not carried out in this study, if the temperature was increased greater than 140 °C, the QE may saturate at a maximum value and then begin to decrease past a certain temperature. QE may also have saturated if the device was held at one temperature point for a long time. Such studies would be useful in finding the optimal annealing conditions.

In Fig. 14 the data for the second temperature transition (cooling) is shown, though it is difficult to see in the figure, the wavelength position of the peaks as well as the values of the peaks shifted. The QE peaks near 500 nm showed a 10 nm shift in position from −10 to 140 °C. The wavelength shift in QE clearly followed the shift in absorption of the P3HT/PCBM blend. The short wavelength peaks did not shift position with temperature, which also agrees with absorption data. The change in the peak values of QE near 500 nm are best viewed in Fig. 15, where it can be seen that the peak QE increases with temperature until 60 °C, at which it reaches the maximum and further decreases at high temperatures. To understand this behavior, we must examine the factors that affect QE. QE is dependent on current; therefore, it is dependent on the absorption and the conductivity of the film. Absorption was always higher at lower temperatures, which would cause the QE peaks to be higher at lower temperatures; however, studies on the hole mobility of P3HT have shown that it generally rises with temperature because the transport is based on hopping of electrons and holes, instead of band transport [14,24]. In one study, the mobility was found to rise until around 80 °C at which a plateau formed [15]. In another study, mobility rose until 107 °C at which it began to decrease, which was attributed to morphology defects at high temperatures [14]. We found that PL intensity was higher at low temperatures because of less non-radiative recombination. The QE behavior can be explained by the competing effects of absorption, mobility, and recombination. Absorption and photoluminescence were both higher at low temperatures; however, as shown in literature, the mobility of P3HT increases with increasing temperature to some point [15,16]. QE should increase with increase in mobility due to higher conductivity. All these factors interact and affect the QE of a device, which can explain the maximum QE near the middle of the temperature range.

Once annealed, all the samples followed the behavior shown in Figs. 14 and 15, and the temperature effects were reversible.

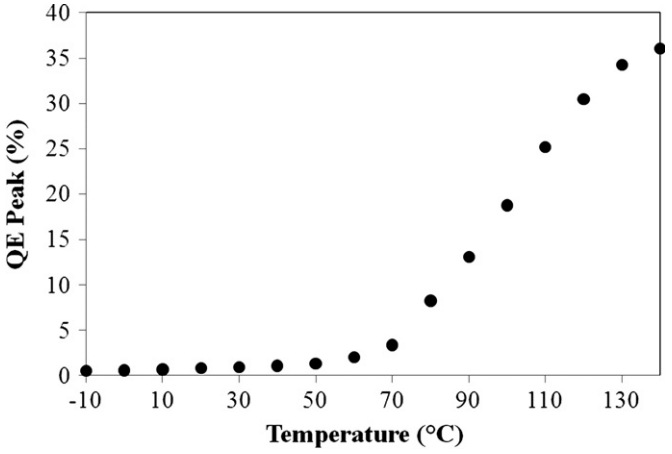

Fig. 13. Unannealed device peak QE, first temperature transition, heating from −10 to 140 °C.

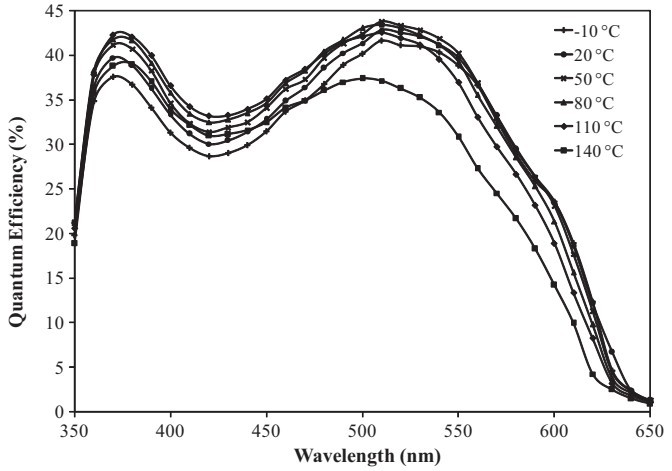

Fig. 14. Unannealed device QE, second temperature transition, cooling from 140 to −10 °C.

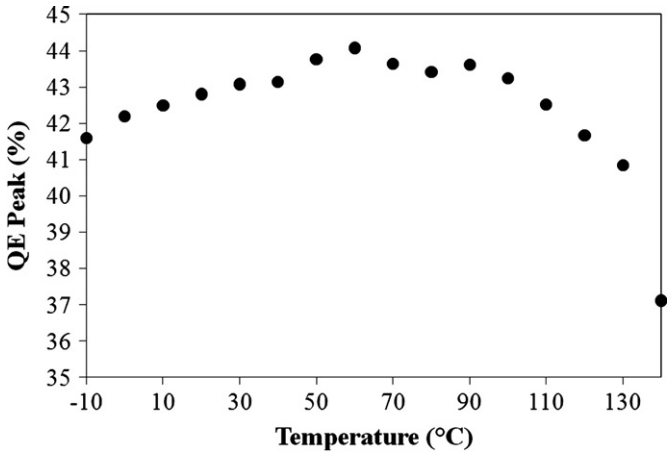

Fig. 15. Unannealed device peak QE, second temperature transition, cooling from 140 to −10 °C.

3.4. Total efficiency and I–V parameters

The control device showed a decrease in open circuit voltage, short circuit current density, fill factor, and total efficiency due to repeated exposure of intense light. After being illuminated for the same amount of time as the experimental samples, open circuit voltage of the control device decreased by less than 1% (0.645–0.640 V). Short circuit current density decreased by less than 5% (4.8–4.7 mA/cm^2) Fill factor decreased by less than 3% (54.4%–53.1%). Total efficiency decreased by less than 8% (1.73%–1.60%).

3.4.1. Unannealed P3HT/PCBM device

I–V parameters for the unannealed P3HT/PCBM device during the first temperature transition (heating) are shown in Fig. 16. On heating the device all parameters increased with temperature. The maximum efficiency, short circuit density, open circuit voltage, and fill factor all occurred at 140 °C. The increase in all the parameters with temperature can be attributed to the increase in crystallinity and mobility of the film as it was heated. The increase in J_{sc} very closely resembles the increase in the peak QE of the unannealed device shown in Fig. 13, which is expected. It is interesting to note

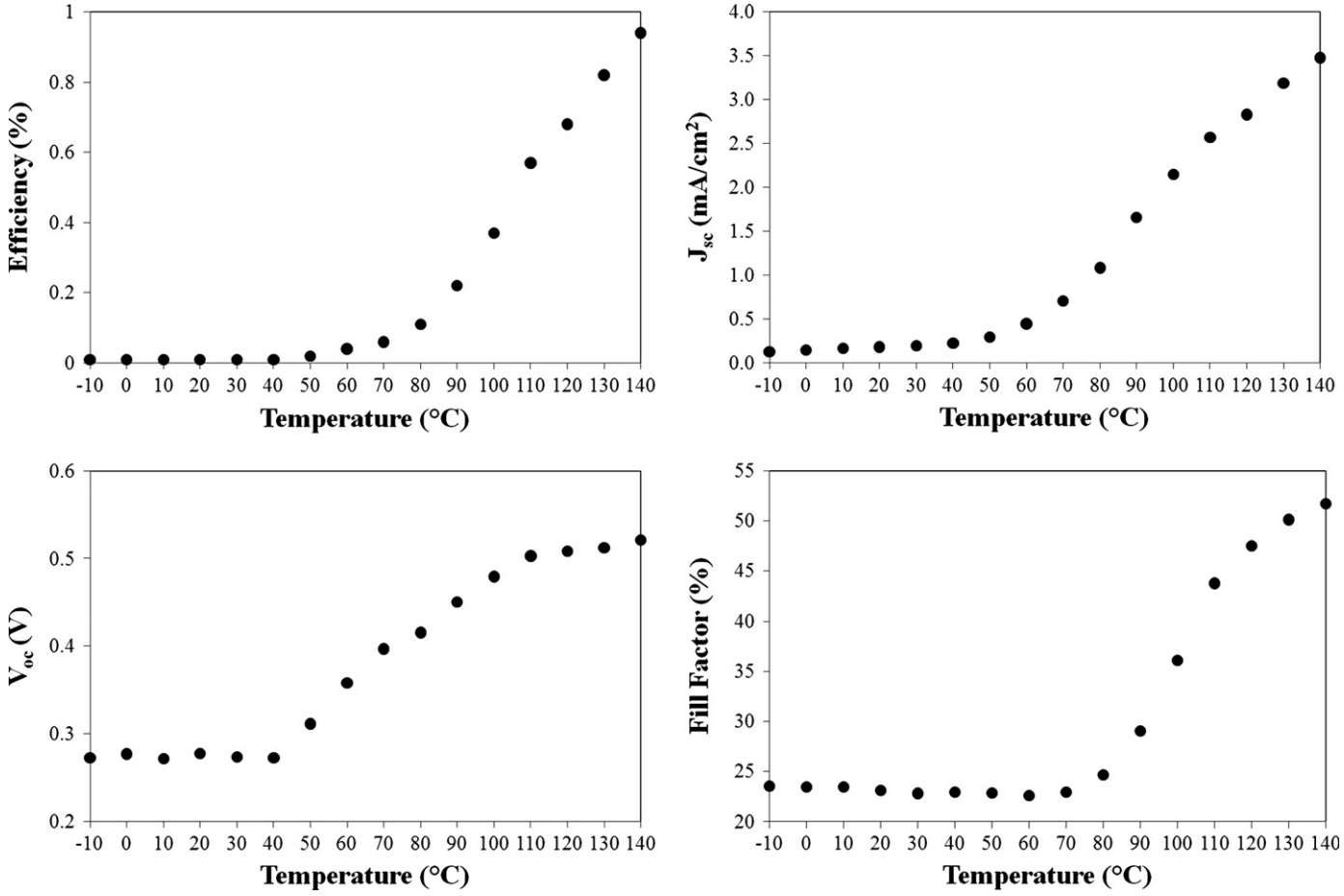

Fig. 16. Unannealed device performance, first temperature transition, heating from −10 to 140 °C.

that open circuit voltage began to increase at a much lower temperature than other parameters. Monitoring efficiency during annealing could be used to find optimal annealing conditions; however, degradation due to intense light needs to be considered.

I–V parameters for the unannealed P3HT/PCBM device during the second temperature transition (cooling) are shown in Fig. 17. On cooling the device the maximum efficiency of 1.39% was obtained at 20 °C; maximum current density of 4.2 mA/cm^2 was obtained at 60 °C. Open circuit voltage increased linearly with decreasing temperature and reached the maximum of 0.668 V at −10 °C. The maximum fill factor of 53.40% occurred at 80 °C. The current also resembled the change in QE peaks as shown in Fig. 15.

During the third temperature transition (the second heating) the unannealed samples followed the behavior shown in Fig. 17. The annealed samples followed the behavior shown in Fig. 17 during all the temperature transitions. The behavior was reversible and repeatable, except for a small amount of degradation, which was similar to that of the control samples.

The *I–V* data followed the same trends as in literature; however, maximum values were obtained at different temperatures. In the work reported by Chirvase et al. [18], the short circuit current peak occurred at 27 °C and the efficiency and FF at 47 °C . In our study, using two different devices over a total of 5 measurements, the average temperature for maximum efficiency was 26 °C, maximum short circuit current density was at 50 °C, and maximum fill factor was at 94 °C. Open circuit voltage was always highest at −10 °C. One reason for the discrepancy could be that in the work reported by Chirvase et al. [18], the total efficiency was only around 0.1% at room temperature where our efficiencies were of the order of ten times higher. In the work by Krebs et al. [11], efficiency peak occurred at 40 °C, current at 90 °C, voltage at −30 °C, and FF from 40 to 70 °C. A key difference is that these devices were encapsulated, thus limiting the degradation in high temperatures due to exposure to air.

We now have a better picture of the temperature dependence of organic solar cells. Changes in absorption are expected due to changes in conjugation of the polymer units. Changes in PL are due to changes in conjugation as well as higher recombination at high temperatures due to increased defect density or thermal noise. Short circuit current variation is mainly due to variation in mobility with temperature; however, variation in absorption with temperature will also play a small role. Quantum efficiency depends on changes in current as well as absorption. The linear decrease in open circuit voltage with increasing temperature has been discussed in literature, but is not fully theoretically understood [25,26]. This may also be due to changes in energy level positions with temperature as indicated from absorption and photoluminescence data. Further investigation of these effects may lead to a better understanding of the origin of open circuit voltage in organic solar cells. Fill factor depends on current, voltage, and conductivity, and its behavior is a sum of those behaviors. Changes in morphology may also play a role. The combined effects of short circuit current, open circuit voltage, and fill factor lead to the behavior of total efficiency.

4. Conclusions

A method and apparatus for evaluating various parameters of P3HT, PCBM, and P3HT/PCBM organic solar cells at temperatures

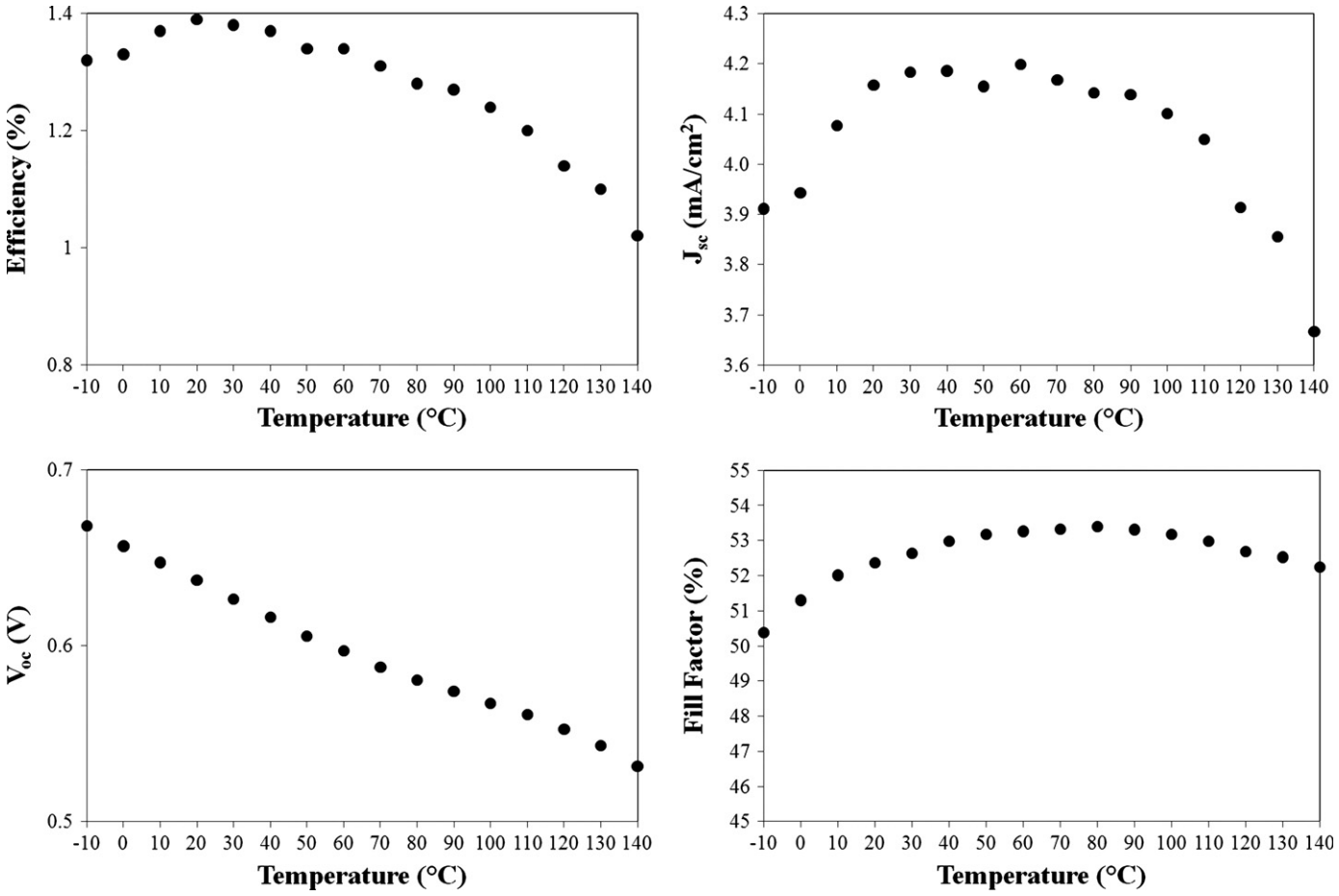

Fig. 17. Unannealed device performance, second temperature transition, cooling from 140 to −10 °C.

from −10 to 140 °C were developed. Light absorption, photoluminescence, quantum efficiency, *I–V* parameters, and total efficiency were measured in the temperature range.

Absorption of devices increased with annealing. Once fully annealed, the P3HT/PCBM blend showed reversible changes with temperature that followed pure P3HT due to conformation defects in the polymer. PL of the blend increased with annealing. Annealed devices showed reversible changes with temperature that followed pure P3HT. PL quenching was not temperature dependent. The PL measurements were shown to be more sensitive to annealing than that of the absorption measurements. Monitoring PL intensity may be the best way to monitor the annealing process without fabricating a full device.

Quantum efficiency of device rose drastically with increasing temperature as the devices became annealed. After the initial heating, QE showed the same peak shifts as the P3HT/PCBM blend showed in absorption. The changes in the magnitude of the QE peaks with temperature were explained by the competing effects of absorption, mobility, and recombination with temperature. *I–V* characteristics of unannealed devices increased with annealing and varied with temperature after annealing. Efficiency peak occurred at an average temperature of 26 °C. Real world performance of devices would be best around room temperatures.

Possible future studies include the temperature dependence of mobility of the P3HT/PCBM blend, temperature dependence of morphology of the materials and devices, and temperature dependence of degradation. The method described could be used to study new material systems, including determining optimal annealing temperature and time. Efficiency and other parameters could be monitored during the annealing process to see at which temperature the maxima occur. The temperature could be held constant and measurements could be taken over time to find an optimal annealing time.

Acknowledgements

We would like to thank the NASA Langley Professor program and the NSF I/UCRC program for their financial support.

References

[1] A.C. Mayer, S.R. Scully, B.E. Hardin, M.W. Rowell, M.D. McGehee, Polymer-based solar cells, Mater. Today 10 (2007) 28–33.
[2] F.C. Krebs, S.A. Gevorgyan, J. Alstrup, A roll-to-roll process to flexible polymer solar cells: model studies, manufacture and operational stability studies, J. Mater. Chem. 19 (2009) 5442–5451.
[3] F.C. Krebs, T. Tromholt, M. Jørgensen, Upscaling of polymer solar cell fabrication using full roll-to-roll processing, Nanoscale 2 (2010) 873–886.
[4] F.C. Krebs, K. Norrman, Using light-induced thermocleavage in a roll-to-roll process for polymer solar cells, ACS Appl. Mater. Interfaces 2 (2010) 877–887.
[5] F.C. Krebs, T.D. Nielsen, J. Fyenbo, M. Wadstrømc, M.S. Pedersen, Manufacture, integration and demonstration of polymer solar cells in a lamp for the "Lighting Africa" initiative, Energy Environ. Sci. 3 (2010) 512–525.
[6] A.J. Medford, M.R. Lilliedal, M. Jørgensen, D. Aarø, H. Pakalski, J. Fyenbo, F.C. Krebs, Grid-connected polymer solar panels: initial considerations of cost, lifetime, and practicality, Opt. Express. 18 (S3) (2010) A272–A285.
[7] F.C. Krebs, J. Fyenbob, M. Jørgensen, Product integration of compact roll-to-roll processed polymer solar cell modules: methods and manufacture using flexographic printing, slot-die coating and rotary screen printing, J. Mater. Chem. (2010). doi:10.1039/C0JM01178A Advance article.
[8] G. Li, V. Shrotriya, J. Huang, Y. Yao, T. Moriarty, K. Emery, Y. Yang, High-efficiency solution processable polymer photovoltaic cells by self-organization of polymer blends, Nat. Mater. 4 (2005) 864–868.

[9] W. Ma, C. Yang, X. Gong, K. Lee, A.J. Heeger, Thermally stable, efficient polymer solar cells with nanoscale control of the interpenetrating network morphology, Adv. Funct. Mater. 15 (2005) 1617–1622.
[10] Y. Kim, S. Cook, S.M. Tuladhar, S.A. Choulis, J. Nelson, J.R. Durrant, D.D.C. Bradley, M. Giles, I. McCulloch, C. Ha, M. Ree, A strong regioregularity effect in self-organizing conjugated polymer films and high-efficiency polythiophene:fullerene solar cells, Nat. Mater. 5 (2006) 197–203.
[11] F.C. Krebs, et al., A round robin study of flexible large-area roll-to-roll processed polymer solar cell modules, Sol. Energy Mater. Sol. Cells 93 (2009) 1968–1977.
[12] M. Helgesen, R. Søndergaard, F.C. Krebs, Advanced materials and processes for polymer solar cell devices, J. Mater. Chem. 20 (2010) 36–60.
[13] O. Inganas, W.R. Salaneck, J.E. Osterholm, J. Laakso, Thermochromic and solvatochromic effects in poly(3-hexylthiophene), Synth. Metals 22 (1988) 395–406.
[14] S. Grecu, M. Roggenbuck, A. Opitz, W. Brutting, Differences of interface and bulk transport properties in polymer field-effect devices, Org. Electron. 7 (2006) 276–286.
[15] Z. Chiguvare, V. Dyakonov, Trap-limited hole mobility in semiconducting poly(3-hexylthiophene), Phys. Rev. B Condens. Matter 70 (2004) 235207-1–235207-8.
[16] L.A. Majewski, R. Schroeder, M. Grell, P.A. Glarvey, M.L. Turner, High capacitance organic field-effect transistors with modified gate insulator surface, J. Appl. Phys. 96 (2004) 5781–5787.
[17] P.J. Brown, D.S. Thomas, A. Köhler, J.S. Wilson, J.S. Kim, C.M. Ramsdale, H. Sirringhaus, R.H. Friend, Effect of interchain interactions on the absorption and emission of poly(3-hexylthiophene), Phys. Rev. B Condens. Matter 67 (2003) 064203-1–064203-16.
[18] D. Chirvase, Z. Chiguvare, M. Knipper, J. Parisi, V. Dyakonov, J.C. Hummelen, Temperature dependent characteristics of poly(3 hexylthiophene)-fullerene based heterojunction organic solar cells, J. Appl. Phys. 93 (2003) 3376–3383.
[19] Y. Kim, S.A. Choulis, J. Nelson, D.D.C. Bradley, Composition and annealing effects in polythiophene/fullerene solar cells, J. Mater. Sci. 40 (2005) 1371–1376.
[20] G. Li, V. Shrotriya, Y. Yao, J. Huanga, Y. Yang, Manipulating regioregular poly (3-hexylthiophene):[6,6]-phenyl-C61-butyric acid methyl ester blends—route towards high efficiency polymer solar cells, J. Mater. Chem. 17 (2007) 3126–3140.
[21] Y. Kim, S.A. Choulis, J. Nelson, D.D.C. Bradley, S. Cook, J.R. Durrant, Device annealing effect in organic solar cells with blends of regioregular poly (3-hexylthiophene) and soluble fullerene, Appl. Phys. Lett. 86 (2005) 063502-1–063502-3.
[22] R. Cugola, U. Giovanella, P. Di Gianvincenzo, F. Bertini, M. Catellani, S. Luzzati, Thermal characterization and annealing effects of polythiophene/fullerene photoactive layers for solar cells, Thin Solid Films 511–512 (2006) 489–493.
[23] D. Chirvase, J. Parisi, J.C. Hummelen, V. Dyakonov, Influence of nanomorphology on the photovoltaic action of polymer–fullerene composites, Nanotechnology 15 (2004) 1317–1323.
[24] A. Zen, J. Pflaum, S. Hirschmann, W. Zhuang, F. Jaiser, U. Asawapirom, J.P. Rabe, U. Scherf, D. Neher, Effect of molecular weight and annealing of poly (3-hexylthiophene)s on the performance of organic field-effect transistors, Adv. Funct. Mater. 14 (2004) 757–764.
[25] F. Belhocine-Nemmar, M.S. Belkaid, D. Hatem, O. Boughias, Temperature effect on the organic solar cells parameters, World Acad. Sci. Eng. Technol. 64 (2010) 132–134.
[26] P. Kumar, S.C. Jain, H. Kumar, S. Chand, V. Kumar, Effect of illumination intensity and temperature on open circuit voltage in organic solar cells, Appl. Phys. Lett. 94 (2009) 183505-1–183505-3.